SPECIAL TOPIC — A 40th Anniversary Celebration: Physics Research and Innovation at Ningbo University

Superconductivity of highly hydrogen-rich hydride CsH_{25}

Xiaoyan Yan(严小燕)[1], Hongyu Huang(黄泓瑜)[1], Zhao Liu(刘召)[1,†], Mingyang Du(杜明阳)[1,‡], and Tian Cui(崔田)[1,2]

[1] *Institute of High Pressure Physics, School of Physical Science and Technology, Ningbo University, Ningbo* 315211, *China*
[2] *College of Physics, Jilin University, Changchun* 130012, *China*

(Received 31 May 2026; revised manuscript received 6 July 2026; accepted manuscript online 9 July 2026)

Hydrogen-rich hydrides have been regarded as a crucial framework for achieving high-temperature superconductivity. Here, through random structure search combined with first-principles calculations, we predict a thermodynamically stable hydrogen-rich hydride CsH_{25} in the CsH system within a pressure range of 100–400 GPa. The results demonstrate the presence of quasi-H_2 units embedded within the metallic cesium framework, where alkali metals provide a constant charge and support the hydrogen–cesium alloy framework to maintain a stable crystal structure. This structural feature exerts a significant influence at both the electronic and phononic levels. The synergistic interaction between these electronic and phononic features ultimately enables the system to exhibit a superconducting transition temperature approaching 98 K at 100 GPa. Unlike traditional high-temperature superconductors that rely on complex covalent hydrogen networks, this study demonstrates that in simple binary systems, quasi-molecular hydrogen can also achieve strong electron–phonon coupling by modulating the electronic states at the Fermi level and inducing phonon softening. In systems containing molecular hydrogen units, superconductivity arises from the synergistic regulation of the electronic structure and phonon behavior. This provides novel insights into the superconducting mechanisms in such systems and enriches research on quasi-molecular hydrides.

Keywords: hydrogen-rich hydrides, superconductivity, high pressure

PACS: 74.70.Ad, 74.10.+v, 74.62.Fj

DOI: 10.1088/1674-1056/ae881e **CSTR:** 32038.14.CPB.ae881e

1. Introduction

Since the discovery of superconductivity, its unique properties — such as zero resistance and complete diamagnetism[1] — have endowed it with significant application potential in fields including energy transmission, precision measurement, and quantum information. Researchers are now striving to discover and develop superconductors that operate at higher temperatures, a breakthrough that would revolutionize energy transport and storage. Since Onnes[2] first discovered the superconducting phenomenon, in which metallic mercury (Hg) exhibits zero resistance at 4.2 K in 1911, investigating room-temperature superconductivity has remained one of the most formidable challenges in condensed matter physics and materials science. According to the BCS theory,[3] hydrogen is not only the lightest element but also possesses the highest Debye temperature. In 1968, Ashcroft[4] proposed that metallic hydrogen could become a room-temperature superconductor, however, since the metallization of pure hydrogen typically requires an extremely high pressure exceeding 300 GPa,[5] this process is difficult to achieve. In 2004, to reduce the pressure requirements, he further proposed "the chemical precompression theory":[6] by introducing additional elements into the structure, this method lowers the pressure required for metallization and the superconducting transition, thereby opening a new direction for research on hydride superconductors. Under the guidance of this theory, a wide range of high-pressure binary hydrides has been predicted.[7–14] In 2014, H_3S[15] reached a superconducting transition temperature of 203 K under a pressure of 250 GPa, signifying a notable milestone in high-T_c hydride research. Afterward, binary hydrides such as LaH_{10}[16] also demonstrated outstanding performance. Other binary hydrides have also been experimentally confirmed, such as $ThH_{9,10}$,[17] YH_9,[18,19] CaH_6,[20,21] YH_6,[22] CeH_9,[23] $(La,Y)H_{10}$[24] and $(La,Ce)H_{9,10}$.[25] These systems exhibit excellent superconducting properties under high pressure. These studies have established "high-pressure hydrogen-rich systems" as a critical pathway for achieving high-temperature superconductivity.

Nevertheless, such systems typically require extreme pressure conditions exceeding 100 GPa, severely limiting their experimental feasibility and potential applications. Consequently, achieving high critical temperature (T_c) superconductivity under lower pressures has become a key research focus. In recent years, investigations have expanded from traditional high-pressure binary hydrides to more complex ternary systems, with many low-pressure-stable ternary hydrogen-rich materials exhibiting remarkably high T_c val-

†Corresponding author. E-mail: liuzhao@nbu.edu.cn
‡Corresponding author. E-mail: dumingyang@nbu.edu.cn

© 2026 Chinese Physical Society and IOP Publishing Ltd. All rights, including for text and data mining, AI training, and similar technologies, are reserved.

CPB Online In Press

ues, such as $CaBH_5$ (83 K at 1 GPa),[26] $ThBeH_8$ (113 K at 7 GPa),[27] $LaTh_3H_{24}$ (198 K at 50 GPa),[28] $KGaH_3$ (146 K at 10 GPa),[29] and $RbInH_3$ (130 K at 6 GPa).[29] By modulating the components and structure, the stabilization pressure is reduced while maintaining strong electron–phonon coupling. Among these, the experimental synthesis of $LaBeH_8$[30] marked a significant milestone, achieving a superconducting transition temperature T_c of 110 K under a pressure of 80 GPa.

Currently, nearly all binary hydrides have been extensively studied. However, research on the low-pressure superconductivity of binary hydrides remains relatively limited. Cesium (Cs), a typical alkali metal with a relatively large atomic mass, acts as an outstanding electron donor and improves superconducting performance by substantially adjusting the lattice structure and electron distribution. In 2012, Shamp *et al.*[31] predicted five distinct nearly isenthalpic CsH_3 structures — *Cmmm*, *Cmma*, $I4_1/amd$, $P2c$, and $C2c$ — in his theoretical study of the Cs–H binary system. Among these, $I4_1/amd$ exhibits metallic behavior below 100 GPa and remains stable even at pressures as low as 2 GPa. This discovery fills the theoretical gap in the CsH system under high pressure. Notably, new experimental findings have also been made regarding the CsH system. In 2024, Di Zhou's research group[32] synthesized high-hydrogen compounds such as CsH_7 and CsH_{15+x} using high-pressure DAC technology, which exhibited exceptional stability under low pressure — particularly CsH_7, which remained stable under near-standard environmental conditions. Subsequent studies on the ternary system have also demonstrated that cesium exhibits exceptional stability toward hydrides under near-room-temperature conditions; for example, $CsBH_5$[27] demonstrates excellent thermodynamic stability and potential superconducting properties. In earlier research, $XInH_3$ (where X = K, Rb, Cs)[29] also exhibited outstanding superconducting performance.

Therefore, we selected cesium and hydrogen as the constituent elements, conducted a systematic structural investigation of the Cs–H system, and predicted the formation of a hydrogen-rich compound, CsH_{25}. Unlike traditional cesium hydrides where ionic interactions dominate, this structure features hydrogen units with H_2-like bonding characteristics embedded within the metal matrix, resulting in a structural configuration where H–H covalent bonds coexist with delocalized electronic states. This unique bonding mechanism opens new possibilities for transcending conventional high-temperature superconductivity design approaches reliant on extended hydrogen networks and for investigating superconducting mechanisms in binary hydrogen-rich hydrides. In recent years, hydrogen units that retain limited H–H bonding characteristics in high-pressure hydrides have attracted widespread attention. For example, in systems such as $CsInH_7$ (81 K at 41 GPa),[33] Mg_2AcH_{16} (221 K at 70 GPa),[34] NaH_{10} (270 K at 400 GPa),[35] ScH_{12} (313 K at 90 GPa),[36] BiH_4 (91 K at 170 GPa),[37] $C2/c$-CaH_{14} (204.0 K at 300 GPa),[38] $NaKH_{12}$ (245 K at 60 GPa),[39] the partially preserved H–H pairs or molecular hydrogen fragments are believed to play a crucial role in structural stability and superconducting behavior. Previous studies typically classify these hydrogen configurations as "quasi-molecular hydrogen", characterized by H–H bond lengths ranging between those of free hydrogen molecules and fully dissociated atomic hydrogen, typically around 0.75–1.00 Å. In contrast, CsH_{25} exhibits an H–H bond length of 0.747 Å, nearly identical to that of a free H_2 molecule and significantly shorter than the typical quasi-H_2 molecular bond lengths (0.75–1.00 Å) reported in the above systems, indicating that its H_2 units largely retain the characteristics of free molecules. The electron–phonon coupling behavior of such nearly unperturbed H_2 units in a metallic environment warrants further investigation. Besides, existing theoretical studies on Cs–H systems[31,32] have all focused on low-hydrogen stoichiometric structures ranging from CsH to CsH_{16}. Distinct from all previously reported cesium hydrides, the CsH_{25} phase possesses a hydrogen-to-metal ratio of 25. Its unique structural configuration, where molecular H_2 coexists with free H^- anions within the crystal lattice, provides a distinctive platform for exploring the interplay between molecular and ionic hydrogen. During the preparation of this manuscript, we became aware of the independent structure prediction of CsH_{25} by Lewis *et al.*,[40] who reported an identical crystal structure using data-driven accelerated crystal structure prediction methods.

Building on these advancements, this study conducts an in-depth investigation of the CsH system using the random structural search (AIRSS) methodology. Within this framework, we have predicted a hydrogen-rich compound, CsH_{25}, whose structure incorporates quasi-H_2 molecular units that play a pivotal role in the metallic environment, facilitating the realization of superconducting properties. Its unique H–H bonding mechanism and behavior under metallic conditions offer a novel perspective for quasi-molecular hydrogen research. Thus, this work not only expands the structural diversity of hydrogen-rich systems containing H–H bond units, but also further enriches the research landscape of quasi-molecular hydrogen-related systems, while providing a physical framework for understanding superconducting behavior in unconventional hydrogen sub-lattices. It is noteworthy that CsH_{25} exhibits a superconducting transition temperature of approximately 97.9 K at 100 GPa, further enriching the theoretical framework of hydride superconductivity and providing insightful design concepts and theoretical foundations for developing high-performance superconducting materials at low pressures.

CPB Online In Press

2. Computational methods

The initial structural exploration of CsH_{25} employed the Ab Initio Random Structure Search (AIRSS) method,[41,42] combined with CASTEP software[43] for local geometric optimization. The stoichiometric ratios of $Cs_{1-4}H_{1-120}$ in the Cs–H binary system were investigated. Approximately 18000 random structures were generated and subjected to structural relaxation at target pressures of 100, 200, 300, 400, and 500 GPa, using a plane-wave truncation energy of 300 eV and a Monkhorst–Pack k-point grid density of $2\pi \times 0.07$ Å^{-1}. The exchange-correlation interactions were calculated using the Perdew–Burke–Ernzerhof (PBE) functional[44] within the framework of the generalized gradient approximation (GGA). To ensure the reliability of the candidate structures, symmetry analysis and enthalpy comparisons were performed to eliminate redundant configurations.

Following the first-principles computations, including crystal structure optimization, electronic structure analysis, and evaluation of thermodynamic properties, all calculations were performed using the Vienna *Ab Initio* Simulation Package (VASP).[45] The projector augmented-wave (PAW) method[46] was employed, with a plane-wave truncation energy set to 700 eV. The Brillouin zone sampling utilized a Γ-centered k-point grid at a density of $2\pi \times 0.03$ Å^{-1}. The valence electron configuration of Cs was explicitly defined as $5s^2 5p^6$, while that of hydrogen was $1s^1$. The energy convergence threshold for all calculations was set below 1 meV/atom.

The calculation of phonon dispersion spectra and electron–phonon coupling matrices was performed using the Quantum ESPRESSO (QE) software package.[47] Ultrasoft pseudopotentials were used, with a plane-wave truncation energy of 100 Ry. For the $Fm\bar{3}c$ CsH_{25} phase, which exhibits dynamic stability under high pressure, an $8 \times 8 \times 8$ k-point grid and a $2 \times 2 \times 2$ q-point grid were employed.[48] The superconducting transition temperature was calculated using the McMillan–Allen–Dynes formula.[49,50]

3. Results and discussion

Here, our comprehensive random structural search for the CsH system identified a highly hydrogen-rich hydride compound, CsH_{25}. To determine the thermodynamic stability of the predicted structures, the candidate structures for each stoichiometric ratio were calculated at pressures of 100, 200, 300, 400, and 500 GPa. Considering that CsH_3 is the most stable phase throughout the entire pressure range of the study, these calculations were performed relative to the standard formation enthalpies of CsH_3 and H_2: $I4_1/amd$ for CsH_3 and $Cmca$ for H_2, representing the stable structures under various pressures:

$$CsH_3 + \frac{n-3}{2}H_2 \rightarrow CsH_n.$$

The results demonstrate that CsH_{25} lies on the convex hull from 100 to 400 GPa (Fig. 1(a)), and it is thermodynamically stable against decomposition into other cesium hydrides and hydrogen over a broad pressure interval. The convex-hull results also reveal a pressure-dependent evolution of the competing phases: CsH_7 is stable at lower pressures, while CsH_{11} and CsH_{15} become favorable with further compression. However, CsH_{25} is lifted above the hull at 500 GPa, indicating that its thermodynamic stability is lost at still higher pressure. Since zero-point energy (ZPE) can make a non-negligible contribution to the energetics of hydrogen-rich compounds, we further constructed ZPE-corrected convex hulls. As shown in Fig. 1(b), CsH_{25} remains on the hull throughout 100–400 GPa after including ZPE, confirming that its stability is robust. At 500 GPa, the ZPE correction does not bring CsH_{25} back onto the convex hull; instead, it increases the distance to the hull from 14.428 meV/atom (without ZPE) to 17.106 meV/atom (with ZPE), further confirming that thermodynamic stability is limited to the 100–400 GPa range. This wide pressure stability range, together with its exceptionally high hydrogen content, makes $Fm\bar{3}c$ CsH_{25} a particularly intriguing phase and naturally motivates a closer examination of its crystal structure. To further verify the robustness of this result, we also constructed the convex hull using elemental Cs and H_2 as reference phases, a more conventional choice that facilitates direct comparison with other hydride systems. As shown in Fig. S1, CsH_{25} remains on the convex hull from 100 to 400 GPa in the static-lattice calculations without ZPE, confirming that its thermodynamic stability is independent of the choice of reference phases. The competing phases identified in the main convex-hull analysis (CsH_7, CsH_{15}) also appear naturally on the elemental-reference hull, consistent with the pressure-dependent phase evolution discussed above.

Since CsH_{25} remains on the convex hull from 100 to 400 GPa, we further analyzed its crystal structure at 100 GPa to elucidate the atomic arrangement responsible for its remarkable stability. We investigated the symmetry of the crystal structure of CsH_{25} at 100 GPa (Fig. 2(a)). Geometric analysis revealed three crystallographically non-equivalent hydrogen atom sites: H1 (0.40536, 0.59464, -0.15112), H2 (0.23599, -0.23599, 1.03975), and H3 (0.50000, 0.50000, -0.50000). The two nearest hydrogen atoms, H1 and H2, form paired quasi-molecular hydrogen units surrounding Cs (1.25000, 0.2500, 0.25000), with an H–H bond distance of 0.747 Å. H3 exists as isolated hydrogen atoms at sites far from Cs atoms and other quasi-molecular hydrogen units. At 100 GPa, the lattice parameters of CsH_{25} are as follows: $a = b = c = 8.425$ Å, $\alpha = \beta = \gamma = 90°$ (Fig. 2(b)). The atomic arrangement of the cubic cell of CsH_{25} on the (0 0 1) crystal plane (Fig. 2(c)) is also shown, together with the arrangement of H atoms on the (0 0 1) crystal plane (Fig. 2(d)). In this system, the distance be-

CPB Online In-Press

tween intermolecular hydrogen atoms is approximately 0.74–0.75 Å, indicating that hydrogen exists in an H_2-like form. As shown in Table S1, the lattice constant decreases monotonically from 8.425 Å at 100 GPa to 7.120 Å at 400 GPa, corresponding to a volume compression of approximately 40% over this pressure range. The intramolecular H–H distance within the quasi-H_2 units shows a modest compression from 0.747 Å to 0.737 Å, confirming the persistence of molecular H_2 units under compression. Meanwhile, the shortest intermolecular H···H contact decreases from 1.50 Å to 1.19 Å, indicating progressively stronger inter-unit interactions at higher pressures. No symmetry lowering or structural phase transition is observed across this pressure range.

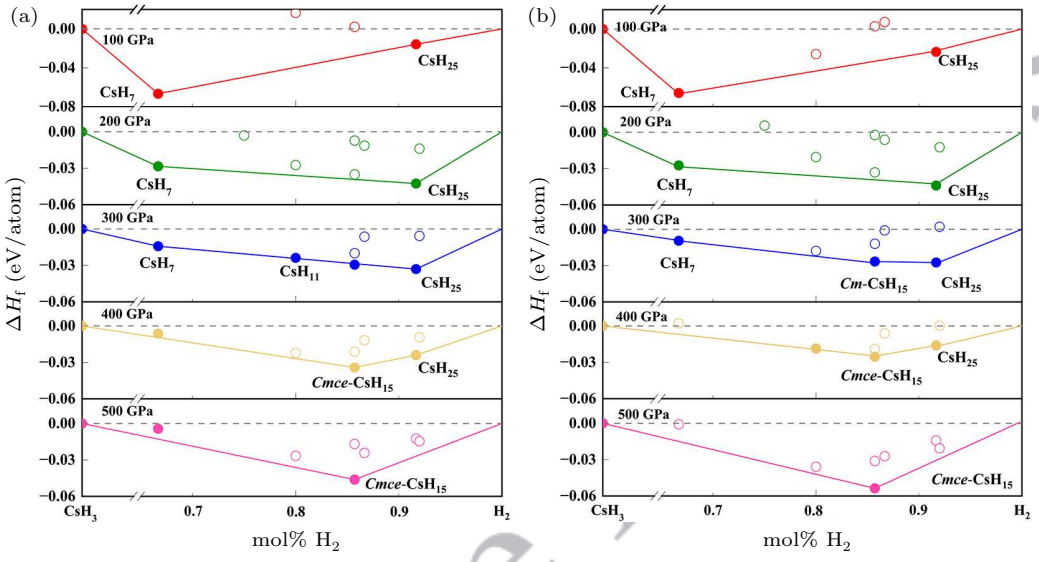


Fig. 1. Formation enthalpies of predicted CsH_n (n = 1–26) with respect to decomposition into CsH_3 and H_2. The $I4_1/amd$ structure for CsH_3 and the *Cmca* structure for H_2 were adopted as the reference structures. (a) Without ZPE and (b) with ZPE included.

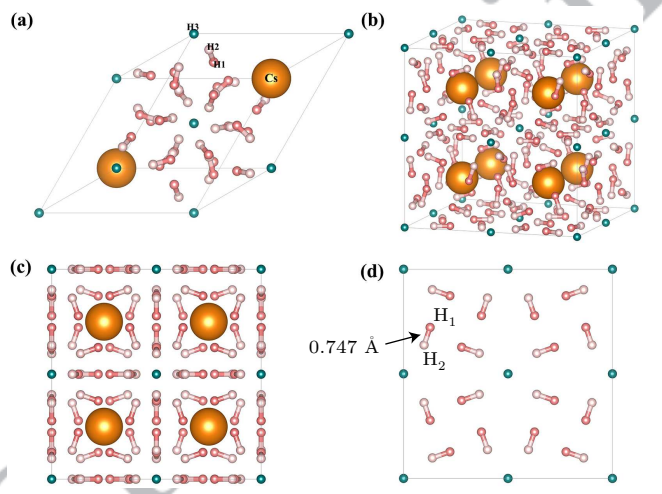


Fig. 2. Three-dimensional structures of $Fm\bar{3}c$ CsH_{25} in (a) the primitive cell and (b) the conventional cell. The large orange sphere represents a Cs atom, while the small green, pink, and red spheres represent different H atoms. (c) Atomic arrangement of the $Fm\bar{3}c$ CsH_{25} conventional cell on the (0 0 1) crystal plane. (d) Arrangement of H atoms on the (0 0 1) crystal plane.

This clear separation between short intramolecular and longer intermolecular H·H distances suggests a well-defined molecular character of hydrogen in the crystal. Therefore, the hydrogen sublattice in CsH_{25} is better described as an assembly of quasi-molecular H_2 units rather than a network of fully dissociated hydride anions. Each H atom is coordinated by two nearest cesium atoms, with all nearest Cs–H distances being 2.359 Å. For each Cs atom, a total of 24 hydrogen atoms is found within a cutoff radius of 2.5 Å, all at the same Cs–H distance of 2.359 Å, indicating a highly symmetric and densely packed hydrogen environment around the cesium centers. Such a coordination pattern suggests that the cesium sublattice provides an extended electrostatic framework that stabilizes the high-hydrogen-content motif.

To further analyze its electron localization, we calculated the two-dimensional electron localization function (ELF) of CsH_{25} across different crystal planes at 100 GPa (Fig. 3). As shown in Fig. 3(a), electron localization is notably pronounced around the hydrogen atoms, exhibiting typical characteristics of molecular bonding. In contrast, near the Cs regions, the electrons demonstrate a more delocalized distribution, reflecting metallic characteristics. This indicates the coexistence of localized and delocalized electrons within the system. Electron localization around hydrogen molecules generally hinders the formation of good metallic properties; however, in Fig. 3(b), the electron distribution of CsH_{25} exhibits significant anisotropy on the (0 0 1) crystal plane. This anisotropic distribution reflects the complex interactions between hydrogen and the metal environment and also provides a physical basis for the subsequent superconducting behavior of CsH_{25}. Therefore, it is necessary to further analyze the charge distribution and band structure of this system to understand the origin of its electron transport characteristics.

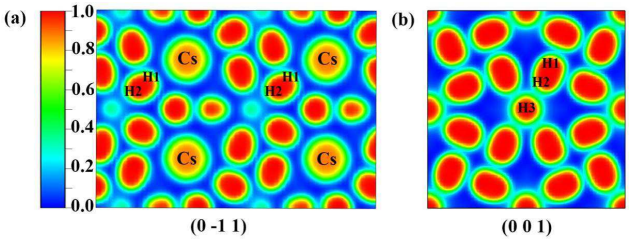


Fig. 3. Two-dimensional electron localization function of $Fm\bar{3}c$ CsH_{25} at 100 GPa on the (a) (0 −1 1) and (b) (0 1) crystal planes, respectively.

To investigate the electronic interactions between Cs and H, we performed a Bader charge analysis (Table 1). The results further corroborate this interpretation. Cs atoms exhibit a Bader charge of 8.221919 e, corresponding to a charge transfer of 0.778081 e, which confirms substantial electron donation from Cs to the hydrogen framework. Most H atoms show Bader charges in the range of 0.98–1.06 e, indicating weak polarization of the molecular-like hydrogen units. In contrast, two H atoms possess a significantly larger Bader charge of 1.365417 e, suggesting the existence of a small number of electronically distinct hydrogen sites. Bader charge analysis further reveals two distinct chemical states of hydrogen in CsH_{25}. Each quasi-H_2 unit consists of two H atoms with net Bader charges of approximately −0.058 e and +0.024 e, reflecting a near-neutral covalent bonding character. The isolated H3 site, however, carries a net Bader charge of −0.365 e, confirming its hydridic H-like nature. These results reinforce the picture of CsH_{25} as a compound containing both molecular H_2 units and isolated hydridic anions. Overall, the combined ELF and Bader results support describing CsH_{25} as a cesium polyhydride composed primarily of quasi-molecular hydrogen units stabilized by an electron-donating Cs framework. However, whether this electronic structure, which preserves the molecular characteristics, can support metallic behavior remains to be further verified.

Table 1. Bader charge analysis of $Fm\bar{3}c$ CsH_{25} at 100 GPa.

Elements	Number of atoms	Structural role	Bader charge (e/atom)	Charge transfer (e/atom)
H1	24	molecular-like H site	∼ 1.06	∼ −0.058
H2	24	molecular-like H site	∼ 0.98	∼ +0.024
H3	2	electronically distinct H site	1.365417	−0.365417
Cs	2	electron donor framework site	8.221919	+0.778081

(–): Indicates that the atom has gained an electron. (+): Indicates that the atom has lost an electron. The values for H1–H3 are given as representative ranges because the symmetry-expanded H atoms show slightly different local Bader charges.

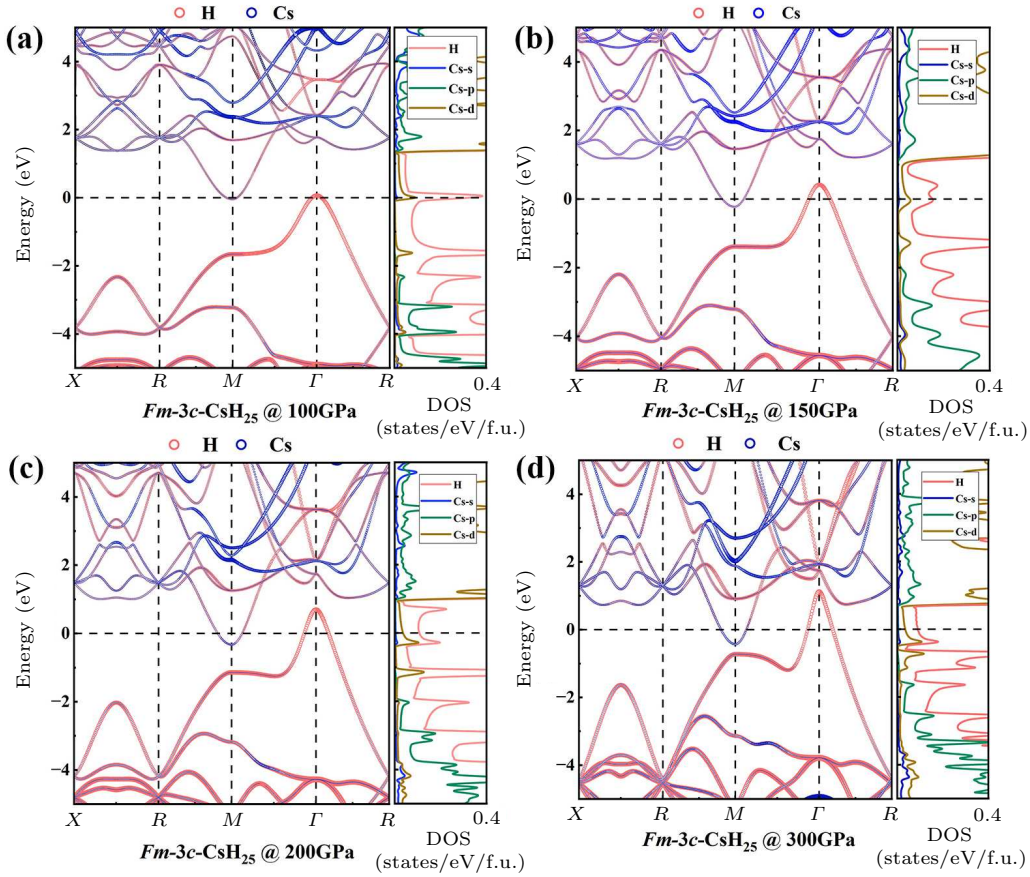


Fig. 4. Electronic band structures and projected density of states (PDOS) of $Fm\bar{3}c$ CsH_{25} at (a) 100 GPa, (b) 150 GPa, (c) 200 GPa, and (d) 300 GPa.

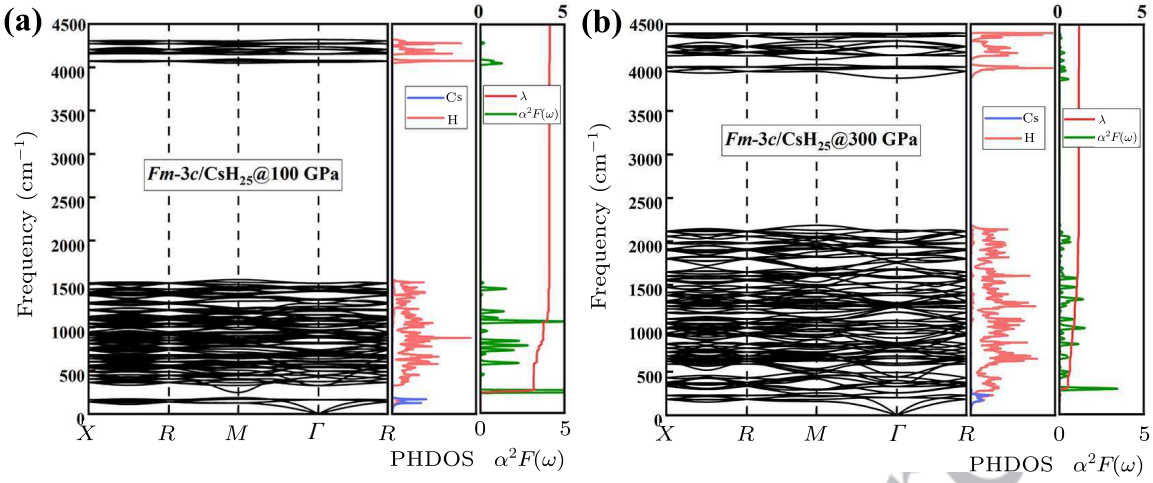


Fig. 5. Calculated phonon band structures, projected phonon density of states (PHDOS), electron–phonon coupling (EPC) parameter λ, and Eliashberg spectral function $\alpha^2F(\omega)$ for CsH_{25} at (a) 100 GPa and (b) 300 GPa.

Building on this foundation, we further calculated the electronic band structures and projected density of states (PDOS) of CsH_{25} under varying pressures (Fig. 4) to investigate the electronic properties of $Fm\bar{3}c$ CsH_{25}. The results demonstrate that a dispersive band crosses the Fermi level at 100 GPa, indicating that CsH_{25} exhibits metallic behavior. The orbital-projected band structure and PDOS further show that the electronic states near the Fermi level are dominated by hydrogen, together with additional contributions from Cs orbitals, suggesting appreciable H–Cs hybridization in the states relevant to electrical transport. Meanwhile, the density of states at the Fermi level is finite but relatively low, implying a weak metallic character rather than a highly conductive metallic state. With increasing pressure from 150 to 300 GPa, no band gap opens, and the metallic nature of CsH_{25} is preserved. At the same time, the bands around the Fermi level gradually evolve under compression, accompanied by changes in the relative contributions of H and Cs states in the PDOS. These results indicate that the hydrogen-rich framework plays a central role in shaping the electronic properties of CsH_{25}, while the availability of H-derived states near the Fermi level provides a favorable electronic basis for the electron–phonon coupling and superconductivity discussed below.

To gain a deeper understanding of the origin of superconductivity in CsH_{25}, we carried out comprehensive first-principles and electron–phonon coupling (EPC) calculations to systematically compare the superconducting and vibrational properties at 100 GPa and 300 GPa. The calculated phonon dispersion relations, projected phonon density of states (PHDOS), and Eliashberg spectral function $\alpha^2F(\omega)$ under both pressure conditions are illustrated in Figs. 5(a) and 5(b), respectively. The entire phonon manifolds at 100 GPa and 300 GPa are free of imaginary vibrational frequencies, verifying that the crystal structure of CsH_{25} retains dynamical stability across this broad pressure window. The softened hydrogen modes strongly couple to hydrogen-derived electronic states at the Fermi level, substantially enhancing the overall EPC strength and serving as a dominant contributor to the large coupling constant λ.

We conducted an in-depth investigation into the pressure dependence of superconductivity based on the complete EPC data of CsH_{25} at 100 and 300 GPa (Table S3). At 100 GPa, the system exhibits a total λ of 4.13, $\omega_{\log}$ of 483.02 K, and T_c of 97.9 K ($\mu^* = 0.1$); at 300 GPa, λ decreases to 1.16, $\omega_{\log}$ increases to 837.63 K, and T_c decreases to 71.8 K. The reduction in λ is attributed to the pressure-induced decrease in $N(E_F)$ from 0.93 to 0.88 states/eV/f.u., which is associated with band broadening, while the increase in $\omega_{\log}$ reflects the overall stiffening of phonon frequencies under compression. The net decrease in T_c indicates that the suppression of λ dominates over the enhancement of $\omega_{\log}$. These results suggest that the superconducting properties of CsH_{25} are stronger at relatively lower pressures within its stability field.

Integrated with our electronic structure calculations, which confirm abundant hydrogen-derived electronic states near the Fermi level, the comparative results at the two pressure points collectively demonstrate that hydrogen species play a pivotal role in both the electronic states and vibrational modes governing superconductivity. Accordingly, the moderately high T_c of CsH_{25} originates from the synergistic coupling between hydrogen-dominated electronic states near the Fermi level and softened hydrogen vibrational modes distributed over the mid-frequency range. At 300 GPa, the disappearance of hydrogen-mode softening and the shift of the $\alpha^2F(\omega)$ peak toward higher frequencies weaken this synergistic interplay, providing a clear microscopic rationale for the reduction of T_c with increasing pressure.

CPB Online in Press

4. Conclusion

Through structural prediction and first-principles calculations, this paper systematically investigates the structural stability, electronic structure, and superconducting properties of the hydrogen-rich compound CsH_{25}. Unlike traditional high-temperature superconductors that rely on extended hydrogen networks, this system contains H_2-like quasi-molecular units with bond lengths comparable to those of free hydrogen molecules. Electronic structure analysis reveals that the system exhibits weak metallic behavior, with electronic states near the Fermi level predominantly originating from hydrogen and exhibiting localized enhancement characteristics. Further analysis combining the electron localization function and charge distribution shows that Cs primarily acts as an electron donor and structural support, without significantly compromising the bonding characteristics of the hydrogen molecular units. Phonon dispersion and electron–phonon coupling calculations demonstrate that the intermediate-frequency hydrogen vibrational modes exhibit pronounced phonon softening, which plays a dominant role in the electron–phonon coupling constant λ. This phonon softening is strongly coupled with the enhanced electronic states near the Fermi level, synergistically enhancing electron–phonon interactions and resulting in a superconducting transition temperature of approximately 97.9 K at 100 GPa. This study demonstrates that in metallic environments, quasi-molecular hydrogen not only exists stably but also enables efficient electron–phonon coupling by modulating Fermi-level electronic states and phonon softening, thereby driving superconductivity. This mechanism provides a physical framework for understanding superconducting behavior in systems containing molecular hydrogen units, expands design approaches for superconducting hydrides, and enriches research on quasi-molecular hydrides.

Acknowledgments

Project supported by the National Key Research and Development Program of China (Grant Nos. 2022YFA1402304 and 2023YFA1406200), the National Natural Science Foundation of China (Grant Nos. 52072188, 12122405, 12274169, 12304021, 52072188 and 51632002), the Program for Science and Technology Innovation Team in Zhejiang (Grant No. 2021R01004), the Zhejiang Provincial Natural Science Foundation of China (Grant No. LQ23A040004), the Natural Science Foundation of Ningbo (Grant No. 2022J091), the Program for Changjiang Scholars and Innovative Research Team in University (No. IRT_15R23), and the Fundamental Research Funds for the Provincial Universities of Zhejiang (Grant No. SJLY2023003).

References

[1] García-Tabarés L 2025 *Riv. Nuovo Cimento* **48** 435
[2] Shan P, Ma L and Cheng J 2024 *Natl. Sci. Rev.* **11** nwae003
[3] Bardeen J, Cooper L N and Schrieffer J R 1957 *Phys. Rev.* **106** 162
[4] Ashcroft N W 1968 *Phys. Rev. Lett.* **21** 1748
[5] Ji C, Li B and Luo J 2025 *Nature* **641** 904
[6] Ashcroft N 2004 *Phys. Rev. Lett.* **92** 187002
[7] Wang H, Tse J S, Tanaka K, Iitaka T and Ma Y 2012 *Proc. Natl. Acad. Sci. USA* **109** 6463
[8] Duan D F, Liu Y X, Tian F B, Li D, Huang X L, Zhao Z L, Yu H Y, Liu B B, Tian W J and Cui T 2014 *Sci. Rep.* **4** 6968
[9] Liu H Y, Naumov I I, Hoffmann R, Ashcroft N W and Hemley R J 2017 *Proc. Natl. Acad. Sci. USA* **114** 6990
[10] Peng F, Sun Y, Pickard C J, Needs R J, Wu Q and Ma Y M 2017 *Phys. Rev. Lett.* **119** 107001
[11] Du M, Zhao W, Cui T and Duan D 2022 *J. Phys.: Condens. Matter* **34** 173001
[12] Song H, Zhang Z, Cui T, Pickard C J, Kresin V Z and Duan D 2021 *Chin. Phys. Lett.* **38** 107401
[13] Du M, Song H, Zhang Z, Duan D and Cui T 2022 *Research* **2022** 9784309
[14] Huang H, Deng C, Song H, Du M, Duan D, Liu Y and Cui T 2024 *Sci. Rep.* **14** 10729
[15] Drozdov A P, Eremets M I, Troyan I A, Ksenofontov V and Shylin S I 2015 *Nature* **525** 73
[16] Drozdov A P, Kong P P, Minkov V S, Besedin S P, Kuzovnikov M A, Mozaffari S, Balicas L, Balakirev F F, Graf D E, Prakapenka V B, Greenberg E, Knyazev D A, Tkacz M and Eremets M I 2019 *Nature* **569** 528
[17] Semenok D V, Kvashnin A G, Ivanova A G, Svitlyk V, Fominski V Y, Sadakov A V, Sobolevskiy O A, Pudalov V M, Troyan I A and Oganov A R 2020 *Mater. Today* **33** 36
[18] Kong P, Minkov V S, Kuzovnikov M A, Drozdov A P, Besedin S P, Mozaffari S, Balicas L, Balakirev F F, Prakapenka V B, Chariton S, Knyazev D A, Greenberg E and Eremets M I 2021 *Nat. Commun.* **12** 5075
[19] Wang Y, Wang K, Sun Y, Ma L, Wang Y, Zou B, Liu G, Zhou M and Wang H 2022 *Chin. Phys. B* **31** 106201
[20] Ma L, Wang K, Xie Y, Yang X, Wang Y, Zhou M, Liu H, Yu X, Zhao Y, Wang H, Liu G and Ma Y 2022 *Phys. Rev. Lett.* **128** 167001
[21] Li Z, He X, Zhang C and Wang X 2022 *Nat. Commun.* **13** 2863
[22] Troyan I A, Semenok D V, Kvashnin A G, Sadakov A V, Sobolevskiy O A, Pudalov V M, Ivanova A G, Prakapenka V B, Greenberg E, Gavriliuk A G, Lyubutin I S, Struzhkin V V, Bergara A, Errea I, Bianco R, Calandra M, Mauri F, Monacelli L, Akashi R and Oganov A R 2021 *Adv. Mater.* **33** 2006832
[23] Chen W, Semenok D V, Huang X, Shu H, Li X, Duan D, Cui T and Oganov A R 2021 *Phys. Rev. Lett.* **127** 117001
[24] Semenok D V, Troyan I A, Ivanova A G, Kvashnin A G, Kruglov I A, Hanfland M, Sadakov A V, Sobolevskiy O A, Pervakov K S, Lyubutin I S, Glazyrin K V, Giordano N, Karimov D N, Vasiliev A L, Akashi R, Pudalov V M and Oganov A R 2021 *Mater. Today* **48** 18
[25] Chen W, Huang X, Semenok D V, Chen S, Zhou D, Zhang K, Oganov A R and Cui T 2023 *Nat. Commun.* **14** 2660
[26] Gao M, Guo P J, Yang H C, Yan X W, Ma F, Lu Z Y, Xiang T and Lin H Q 2023 *Phys. Rev. B* **107** L180501
[27] Jiang Q, Zhang Z, Song H, Ma Y, Sun Y, Miao M, Cui T and Duan D 2024 *Fundam. Res.* **4** 550
[28] Chen W, Ma T, Huo Z, Yu H, Cui T and Duan D 2024 *Phys. Rev. B* **109** 224505
[29] Du M, Huang H, Zhang Z, Wang M, Song H, Duan D and Cui T 2024 *Adv. Sci.* **4** 550
[30] Song Y, Bi J K, Nakamoto Y, Shimizu K, Liu H Y, Zou B, Liu G T, Wang H W and Ma Y M 2023 *Phys. Rev. Lett.* **130** 266001
[31] Shamp A, Hooper J and Zurek E 2012 *Inorg. Chem.* **51** 10143
[32] Zhou D, Semenok D, Galasso M, Alabarse F G, Sannikov D, Troyan I A, Nakamoto Y, Shimizu K and Oganov A R 2024 *Adv. Energy Mater.* **14** 2400077
[33] Huang H, Wang M, Yan X, Song H, Duan D, Cui T and Du M 2025 *Phys. Rev. B* **111** 224502
[34] Wang M, Deng C, Huang H, Yan X, Suo Y S, Xie N, Li W, Ma S, Du M, Song H, Duan D and Cui T 2026 *Chin. Phys. Lett.* **43** 040713
[35] Liu Z, Li J, Zurek E, Zhuang Q, Liu Y, Yue J, Guo S, Zhang A, Chi Z and Huang X 2024 *Phys. Rev. B* **109** L180501

CPB Online In Press

[36] Zhao W, Ellis A, Duan D, Wang H, Jiang Q, Du M, Cui T and Miao M 2025 *Adv. Funct. Mater.* **35** 2415910
[37] Shan P, Ma L, Yang X, Li M, Liu Z, Hou J, Jiang S, Zhang L, Shi L and Yang P 2025 *J. Am. Chem. Soc.* **147** 4375
[38] Liu P, Zhuang Q, Xu Q, Cui T and Liu Z 2026 *Sci. Adv.* **7** 2040
[39] Jiang Q, Duan D, Song H, Zhang Z, Huo Z, Jiang S, Cui T and Yao Y 2024 *Adv. Sci.* **11** 2405561
[40] Conway L J and Pickard C J 2026 *Ann. Phys.* **538** 2500608
[41] Pickard C J and Needs R J 2006 *Phys. Rev. Lett.* **97** 045504
[42] Pickard C J and Needs R J 2011 *J. Phys.: Condens. Matter* **23** 053201
[43] Clark S J, Segall M D, Pickard C J, Hasnip P J, Probert M J, Refson K and Payne M C 2005 *Z. Kristall.* **220** 567
[44] Perdew J P, Burke K and Ernzerhof M 1996 *Phys. Rev. Lett.* **77** 3865
[45] Kresse G and Furthmüller J 1996 *Phys. Rev. B* **54** 11169
[46] Kresse G and Joubert D 1999 *Phys. Rev. B* **59** 1758
[47] Giannozzi P, Baroni S, Bonini N, Calandra M, Car R, Cavazzoni C, Ceresoli D, Chiarotti G L, Cococcioni M and Dabo I 2009 *J. Phys.: Condens. Matter* **21** 395502
[48] Monkhorst H J and Pack J D 1976 *Phys. Rev. B* **13** 5188
[49] McMillan W L 1968 *Phys. Rev. B* **167** 331
[50] Allen P B and Dynes R C 1975 *Phys. Rev. B* **12** 905

CPB Online In-Press